

Water Resources Research

RESEARCH ARTICLE

10.1029/2021WR030664

Key Points:

- Effect of pore-throat radius distribution and connectivity on scale-dependent permeability is investigated
- Depending on pore-throat radius distribution broadness, permeability may increase or decrease with scale
- The modified finite-size scaling analysis results in perfect collapse in data indicating a quasi-universal trend

Correspondence to:

B. Ghanbarian,
ghanbarian@ksu.edu

Citation:

Ghanbarian, B., Esmailpour, M., Ziff, R. M., & Sahimi, M. (2021). Effect of pore-scale heterogeneity on scale-dependent permeability: Pore-network simulation and finite-size scaling analysis. *Water Resources Research*, 57, e2021WR030664. <https://doi.org/10.1029/2021WR030664>




Received 21 JUN 2021
Accepted 29 NOV 2021

Author Contributions:

Conceptualization: Behzad Ghanbarian, Robert M. Ziff, Muhammad Sahimi
Data curation: Behzad Ghanbarian, Misagh Esmailpour
Formal analysis: Behzad Ghanbarian
Investigation: Behzad Ghanbarian, Misagh Esmailpour
Methodology: Behzad Ghanbarian, Misagh Esmailpour, Robert M. Ziff
Supervision: Behzad Ghanbarian, Robert M. Ziff, Muhammad Sahimi
Validation: Behzad Ghanbarian, Misagh Esmailpour, Muhammad Sahimi
Visualization: Behzad Ghanbarian, Misagh Esmailpour
Writing – original draft: Behzad Ghanbarian, Robert M. Ziff, Muhammad Sahimi
Writing – review & editing: Behzad Ghanbarian, Robert M. Ziff, Muhammad Sahimi

© 2021. American Geophysical Union.
All Rights Reserved.

Effect of Pore-Scale Heterogeneity on Scale-Dependent Permeability: Pore-Network Simulation and Finite-Size Scaling Analysis

Behzad Ghanbarian¹ , Misagh Esmailpour¹, Robert M. Ziff² , and Muhammad Sahimi³ 

¹Porous Media Research Lab, Department of Geology, Kansas State University, Manhattan, KS, USA, ²Center for the Study of Complex Systems and Department of Chemical Engineering, University of Michigan, Ann Arbor, MI, USA, ³Mork Family Department of Chemical Engineering and Materials Science, University of Southern California, Los Angeles, CA, USA

Abstract A long-standing issue in subsurface hydrology and many other related disciplines has been the scaling problem. Although the effect of length scale has been known for years, inconsistent results have been reported in the literature. Experimental data mostly indicate that the permeability k should increase with increasing sample volume, whereas simulations and some theoretical predictions appear to imply the opposite. In this paper, we use the concept of finite-size scaling to propose a vigorous theoretical framework for addressing the effect of length scale on the permeability. We simulate fluid flow in 12 synthetic and 4 Fontainebleau pore networks to investigate the effect of small-scale heterogeneities, such as pore-throat size distribution and pore connectivity. Simulations were carried out for 10 pore coordination numbers, namely, $Z = 1.5, 1.65, 1.75, 2, 3, 3.25, 3.5, 4, 5,$ and 6 . For the synthetic pore networks we find a transition in the scale dependence of the permeability, with our results indicating that the permeability increases with the scale for larger pore coordination numbers, whereas the opposite is true for smaller Z . In Fontainebleau pore networks, on the other hand, the trends are decreasing permeabilities regardless of Z . Although the plot of the permeability versus the network size for each pore network appears scattered, through finite-size scaling analysis the data collapse onto a single quasi-universal curve. Our results demonstrate that finite-size scaling analysis is a powerful approach for addressing the effect of length scale on the permeability.

1. Introduction

Flow and transport in porous media are typically investigated at four main length scales, namely, pore, core, lysimeter, and field scales. Accordingly, a long-standing problem in subsurface hydrology has been relating a property's value at one scale, for example, field, to its value at another scale, such as the core scale. This process, called *scaling*, has been a subject of active research in the past several decades (see, e.g., Das & Hassanizadeh, 2005; Gupta et al., 2012; Hopmans et al., 2002; Jury et al., 2011; Kalma & Sivapalan, 1995; Pachepsky et al., 2003; Sposito, 2008).

The influence of scale has been known for years, and it is well documented that physical and hydraulic properties of soils and rocks, such as porosity (Aslannejad et al., 2017; Ewing et al., 2010; Hewett, 1986; Yoon & Dewers, 2013), surface area (Chen et al., 2015; Han et al., 2016; Ji et al., 2012; Navarre-Sitchler & Brantley, 2007), capillary pressure curve (Ghanbarian et al., 2015; Hirsch & Thompson, 1994; Larson & Morrow, 1981; Tinni et al., 2012), tortuosity (Duda et al., 2011; Ghanbarian et al., 2013; Matyka et al., 2008), permeability (Garbesi et al., 1996; Ghanbarian et al., 2017; Neuman, 1994; Pachepsky et al., 2014; Qian et al., 2007), and dispersivity (Ghanbarian-Alavijeh et al., 2012; Neuman, 2005; Wheatcraft & Tyler, 1988) are scale-dependent.

At the pore and core scales, transport is influenced by small-scale heterogeneities, such as pore space structure, pore connectivity, local mineralogy, and surface roughness. The average pore coordination number is probably one of the simplest concepts to characterize the topology of a pore network. In a disordered irregular pore space, such as natural porous materials, one should define the average pore coordination number as the average number of pore throats connected to a pore body. Jerauld et al. (1984) indicated that if the coordination number of a regular pore network equals the average coordination number of an irregular one, flow and transport properties of the two networks would be identical, as long as their other pore-scale characteristics are the same.

At lysimeter and field scales, however, flow is dominated by large-scale spatial heterogeneities, including the spatial distribution of high- and low-permeability zones and their interconnectivity, as well as fractures, faults, and their orientations. Small-scale heterogeneities are captured by experiments or image analyses. For example, direct measurement of pore-space characteristics has substantially advanced with the advent of micro- and nano-computed tomography, producing nondestructive 3D images of porous media with uniform resolution in various directions (Arns et al., 2001, 2002; Blunt et al., 2013; Cnudde & Boone, 2013; Wildenschild & Shepard, 2013). Complete characterization of large-scale heterogeneities is, however, difficult due to spatial and temporal variations. Nonetheless, direct core sampling (Rehfeldt et al., 1992; Sudicky, 1986) and indirect geophysical measurements, such as ground-penetrating radar (Hubbard et al., 1997; Lunt et al., 2005), electrical resistivity imaging (Crook et al., 2008; Vanderborght et al., 2005), well logging, and seismic surveys (Avseth et al., 2010; Kirsch, 2006) have been used to characterize aquifers and to better understand subsurface flow and transport in geological formations.

In the literature, inconsistent results have been reported regarding the effect of length scale on hydraulic properties. For example, experimental data from many sources indicate that the permeability would increase with increasing the scale of measurement or sample volume (Pachepsky et al., 2014; Qian et al., 2007; Rovey & Cherkauer, 1995; Schulze-Makuch et al., 1999). However, pore-network modeling (Bernabé et al., 2003; Sahimi et al., 1986) and some theoretical predictions (Davudov & Moghanloo, 2018) appear to imply the opposite. The latter can be understood as being the result of having more frequent tight pores that act as bottlenecks to flow, as the sample size increases. Such contradictory evidence clearly indicates that, despite numerous practical applications and recent progress, we are still far from having a comprehensive understanding of the effect of the length scale, and in particular small- and large-scale heterogeneities distributed over such scales, on fluid flow and transport in soils and rocks. One prime reason for the current knowledge gap in subsurface hydrology and many other related disciplines is the lack of a comprehensive theory for understanding precisely how hydrological and hydrogeological properties vary with scale. Although two approaches from statistical physics, namely, percolation theory and finite-size scaling analysis, provide solid theoretical foundations for addressing the effect of the length scale, such concepts and approaches, particularly finite-size scaling analysis, are relatively new to subsurface hydrology and their concrete applications have been limited. Therefore, the objectives of this study are to, (a) provide a rigorous theoretical foundation for the interpretation of the scale-dependence of the permeability by integrating finite-size scaling and percolation theories; (b) compare the theory with numerical simulations in synthetic and actual pore networks, and (c) address the effect of pore-throat size distribution and pore coordination number, or connectivity, on the scale-dependence of the permeability.

2. Percolation Theory

Percolation theory (Hunt et al., 2014; Hunt & Sahimi, 2017; Sahimi, 1994; Sahimi & Hunt, 2021; Stauffer & Aharony, 1994) provides a rigorous theoretical framework based on statistical physics of disordered media for studying the effect of the interconnectivity and heterogeneity on flow and transport in porous media. A fundamental concept in percolation theory is the existence of a critical occupation fraction p_c below which a network loses its macroscopic connectivity. In the context of flow and transport in porous media, “occupied” means open to flow and transport. That is, a bond is occupied if it is large enough to allow a fluid to pass through it. Thus, bond percolation is a problem in which a bond is either occupied—open to flow—or vacant—closed to fluid flow because its size is too small or, as in two phase flow, is occupied by a second, completely immiscible fluid. Formulated this way, the problem is isomorphic to resistor and pore networks in which the critical fraction of the bonds depends on the coordination number Z of the network, $p_c \approx E/[Z(E - 1)]$ (Vyssotsky et al., 1961) in which E is the Euclidean dimension of the system. For example, for a square network, $E = 2$ and $Z = 4$, and, thus, if the network is infinitely large, $p_c = 0.5$. Although $p_c \approx E/[Z(E - 1)]$ predicts the exact result for the square network, it provides only approximate, albeit accurate, estimates of p_c for other networks and complex porous media. No exact value of the percolation threshold for any three-dimensional network is known. Thus, accurate determination of percolation threshold in three-dimensional porous media is done by numerical simulation.

Perhaps the most important feature of percolation theory is the fact that various morphological, flow, and transport properties near the critical percolation threshold follow power laws. In particular, the correlation length, ξ , and the permeability, k , conform to the following power laws:

$$\xi \propto |p - p_c|^{-\nu}, \quad 0 \leq p \leq 1 \quad (1)$$

$$k \propto (p - p_c)^t, \quad p_c < p \leq 1 \quad (2)$$

where p is the occupation fraction, p_c is the critical occupation fraction, and $\nu \approx 0.88$ is the universal critical exponent in three dimensions (Kozlov & Laguës, 2010; Stauffer & Aharony, 1994).

Below the percolation threshold p_c ($p < p_c$), all clusters of occupied bonds have finite sizes, and there is no macroscopic connectivity and a spanning cluster. At the percolation threshold ($p = p_c$), an incipient infinite (spanning) cluster forms along with other finite clusters, and the mass of the spanning cluster increases with the linear size, L , of the lattice as a power-law, L^{D_f} , in which D_f is the mass fractal dimension of the fractal cluster. Above the percolation threshold ($p > p_c$), there is the incipient infinite cluster, as well as finite clusters, and due to the presence of macroscopic connectivity the system percolates.

The correlation length, ξ , represents the mean size of the clusters of occupied (unoccupied) bonds below (above) the percolation threshold and, therefore, it diverges as the threshold is approached from below or above that point. More importantly, however, it represents the length scale for macroscopic homogeneity of a percolation network: any network or porous medium with linear size larger than the percolation correlation length may be considered as macroscopically homogeneous (though microscopically heterogeneous). Thus, it is similar to the linear size of a representative elementary volume (REV). In fact, when percolation disorder is present, the percolation correlation length and the REV are essentially the same. In Equation 2, t is the critical exponent of the permeability. In contrast to the exponent ν whose value is universal, that is, it depends only on the dimensionality of the system and not its microscopic details, the value of t can, in principle, depend on the broadness of the bond conductance distribution (Feng et al., 1987; Kogut & Straley, 1979) and, thus, its value may depend on the details of the distributions. If the conductance distribution satisfies certain constraints, however, t too is universal (Kogut & Straley, 1979). Sahimi et al. (1983b) argued that if the first inverse moment of conductance distribution, $h(g)$, is finite, the value of the exponent t should be universal, which is about two in three dimensions. The first inverse moment is given by

$$f_{-1} = \int \frac{h(g)}{g} dg \quad (3)$$

If $f_{-1} = \infty$, however, the scaling exponent t would be a function of the details of the structure of $h(g)$. In Equation 3, $h(g)$ can be determined from the pore-throat size distribution, $h(r_t)$, using Poiseuille's law and the relationship $h(g)dg = h(r_t)dr_t$ in which r_t is the pore-throat effective radius. One may calculate the value of f_{-1} by numerically integrating $\frac{h(g)}{g}$ from g_{\min} to g_{\max} where g_{\min} and g_{\max} are, respectively, the minimum and maximum conductances in the pore network.

3. Finite-Size Scaling Analysis

All the percolation properties, including the percolation thresholds, the power laws (Equations 1 and 2), and the critical exponents, are defined for systems that are infinitely large (Stauffer & Aharony, 1994; Sahimi, 1994). In practice, however, sample sizes and simulation domains are of finite extent. In such systems, as p_c is approached, the correlation length ξ eventually exceeds the system's linear size L and, consequently, L becomes the dominant length scale. Fisher (1971) developed a theory for the scaling properties of a finite thermodynamic system near its critical temperature, called finite-size scaling. Since $|p - p_c| \propto \xi^{-\frac{1}{\nu}}$, when ξ exceeds L , one must replace ξ with L . Thus, adopting Fisher's theory for percolation systems implies that permeability of a system of linear size L should be given by (Sahimi, 1994)

$$k = L^{-\frac{t}{\nu}} f[L^{\frac{1}{\nu}}(p - p_c)] \quad (4)$$

where f is a nonsingular function. In the limit $L \rightarrow \infty$, k follows the power law given by Equation 2. At the percolation threshold ($p = p_c$), the permeability becomes independent of p and p_c , and, thus, Equation 4 reduces to the simple power law $k \propto L^{-t/\nu}$. Note the difference between Equations 2 and 4. While the former is strictly valid only near the percolation threshold, the scaling function $f(x)$ in Equation 4 means that it is valid for any p in a network of linear size L .

Finite-size scaling analysis has been successfully used to determine the critical exponents and even the percolation threshold through simulations of finite systems (Sahimi, 2011; Sahimi et al., 1983a) and to scale the accessible fraction of bonds in percolation theory (Kirkpatrick, 1979; Stauffer & Aharony, 1994) and fractured networks (Masihi et al., 2008; Masihi & King, 2007), as well as fluid flow in single fractures (Pastewka et al., 2013; Petrovitch et al., 2013; Pyrak-Nolte & Nolte, 2016). For example, Pyrak-Nolte and Nolte (2016) recently used Monte Carlo simulation to compute the flow rate and fracture-specific stiffness. Using a finite-size scaling approach similar to Equation 4, Pyrak-Nolte and Nolte (2016) demonstrated that there exists a scaling relationship between flow and stiffness for fractures with strongly correlated aperture distributions, which continues to hold for deformed fractures.

In a network of pores, the average pore coordination number is a function of the number of pore throats and pore bodies (Vogel & Roth, 2001). For several two- and three-dimensional regular networks, such as square, hexagonal, triangular, simple cubic, body-centered cubic, and face-centered cubic networks, Bernabé et al. (2010) demonstrated that the occupation probability p is a linear function of the average pore coordination number Z (see their Figure 1). Accordingly, one may replace p and p_c with Z/Z_{\max} and Z_c/Z_{\max} , respectively, in Equation 4, which yields

$$k = L^{-\frac{t}{\nu}} f[L^{\frac{1}{\nu}}(Z - Z_c)/Z_{\max}] \quad (5)$$

where Z_c is the critical pore coordination number whose value in three dimensions is ~ 1.5 (Bernabé et al., 2010), and Z_{\max} is the maximum pore coordination number in the network. For example, $Z_{\max} = 6$ in cubic networks.

4. Details of the Computations

We first describe generation of the pore networks, after which we explain the calculation of their effective permeability, and estimating the value of the critical exponent t .

4.1. Pore Network Model Generation

To construct the pore networks composed of cylindrical pore throats and spherical pore bodies, we used the open-access code developed by Valvatne (2004). The code generates networks based upon the cubic network with a maximum coordination number of 6. Any desired average pore coordination number less than 6 can, however, be achieved by randomly removing pore throats from the network. The pore-throat radii were generated based on a truncated Weibull distribution with two shape parameters, δ and γ , as well as lower and upper bounds on the sizes, which is given by

$$r_t = (r_{\max} - r_{\min})(-\delta \ln[x(1 - e^{(-1/\delta)}) + e^{(-1/\delta)}])^{1/\gamma} + r_{\min} \quad (6)$$

where x is a randomly generated number ($0 < x < 1$), and r_{\min} and r_{\max} are the smallest and largest pore-throat radii, respectively.

The pore-body radii were accordingly determined based on the following relationship (Valvatne, 2004):

$$r_b = \max \left(\zeta \frac{\sum_{i=1}^n r_{ti}}{n}, \max(r_{ti}) \right) \quad (7)$$

in which n is the number of pore throats connected to the same pore body and ζ is an aspect ratio whose distribution follows the truncated Weibull probability density function. We set $\zeta = 0$ meaning that the pore-body radius has the same size as the largest connected pore throat. In the present work, three pore-throat radius ranges, namely, 0.1–10, 1–50, and 10–75 μm were considered in order to generate different levels of pore-scale heterogeneity. Within each range, we used, $\gamma = 12, 18, 24$, and 30, while setting $\delta = 0.2$. Overall, 12 synthetic pore networks with constant pore-throat length of 100 μm were generated; see Table 1. Such networks with $Z = 6$ exhibit trends in the porosity-permeability data similar to consolidated/unconsolidated sands and carbonate rocks (see Figure 4.1 in Esmailpour, 2021). In addition to the 12 synthetic pore networks, we generated four other pore networks based on Fontainebleau sandstone samples reported by Lindquist et al. (2000). Using the pore-body and pore-throat radii, as well as the pore-throat length distributions, we constructed the Fontainebleau pore networks by

Table 1
Salient Properties of the Sixteen Pore Networks Constructed in This Study

Network	r_b (μm)	r_t (μm)	γ	δ	l_t (μm)	ϕ (%)	t
1.1	0.1–10	0.1–10	12	0.2	100	1.6–4.3	1.46
1.2	0.1–10	0.1–10	18	0.2	100	1.7–4.7	1.60
1.3	0.1–10	0.1–10	24	0.2	100	1.8–4.9	1.63
1.4	0.1–10	0.1–10	30	0.2	100	1.8–5.1	1.64
2.1	1–50	1–50	12	0.2	100	16.1–32.1	1.84
2.2	1–50	1–50	18	0.2	100	17.0–34.2	1.80
2.3	1–50	1–50	24	0.2	100	17.4–35.4	1.77
2.4	1–50	1–50	30	0.2	100	17.7–36.1	1.83
3.1	10–75	10–75	12	0.2	100	24.5–43.9	1.79
3.2	10–75	10–75	18	0.2	100	25.5–46.0	1.88
3.3	10–75	10–75	24	0.2	100	26.0–47.1	1.86
3.4	10–75	10–75	30	0.2	100	26.2–47.8	1.77
Fontainebleau 7.5	8–150	5–70	1.05	0.2	35–1000	4.6–7.1	2.40
Fontainebleau 13	8–183	5–70	1.3	0.2	25–1000	7.7–12.0	2.33
Fontainebleau 15	9–150	5–80	1.3	0.2	25–1000	8.1–13.3	2.60
Fontainebleau 22	11–260	4–100	1.3	0.2	10–900	18.4–23.2	2.74

Note. The lower and upper bounds of porosity correspond to $Z = 1.5$ and 6, respectively. r_b is pore-body radius, r_t is pore-throat radius, γ and δ are Weibull distribution parameters, l_t is pore-throat length, ϕ is porosity, and t is the permeability scaling exponent.

matching their porosity at the average pore coordination number, that is, 3.37, 3.49, 3.66, and 3.75, respectively for Fontainebleau 7.5, 13, 15, and 22, reported by Lindquist et al. (2000).

Figures 1 and 2 show, respectively, the pore-body and pore-throat radius distributions for the synthetic and Fontainebleau pore networks. The two distributions become broader as one moves from Network 1 to 3. Although the pore-throat radius spans two order of magnitude variations ($0.1 \leq r_t \leq 10$) in Network 1 (Table 1), the frequencies of smaller pore throats are zero as shown in Figure 2, due to the values of shape parameters γ and δ . Note that the scales on the vertical and horizontal axes are identical for Networks 1–3 in Figures 1 and 2. The four Fontainebleau sandstones have the broadest distributions among all the pore networks generated in this study. We also present in Figure 3 the pore-throat length distribution for each Fontainebleau sandstone. As reported in Table 1, the pore-throat length approximately varied between 10 and 1,000 μm in the Fontainebleau pore networks. For each pore network, we varied the average pore coordination number, $Z = 1.5, 1.65, 1.75, 2, 3, 3.25, 3.5, 4, 5,$ and 6, and the network size, $L = 1,130, 2,250, 3,380, 4,510,$ and 6,770 μm .

4.2. Simulation of Flow in Pore Networks

We simulated fluid flow in the pore networks using the “poreflow” code developed by Valvatne (2004), utilizing periodic boundary conditions. The permeability was determined using Darcy’s law

$$k = \frac{\mu Q L}{A(P_{in} - P_{out})} \quad (8)$$

where A is the network cross-sectional area, μ is the fluid viscosity, L is the network length, Q is the total flow rate, P_{in} is the pressure at the inlet, and P_{out} at the outlet. The total flow rate was calculated by solving for the pressure distribution throughout the network under the steady-state condition, using mass conservation at each pore body (assuming a fluid with constant density):

$$\sum_j q_{ij} = 0 \quad (9)$$

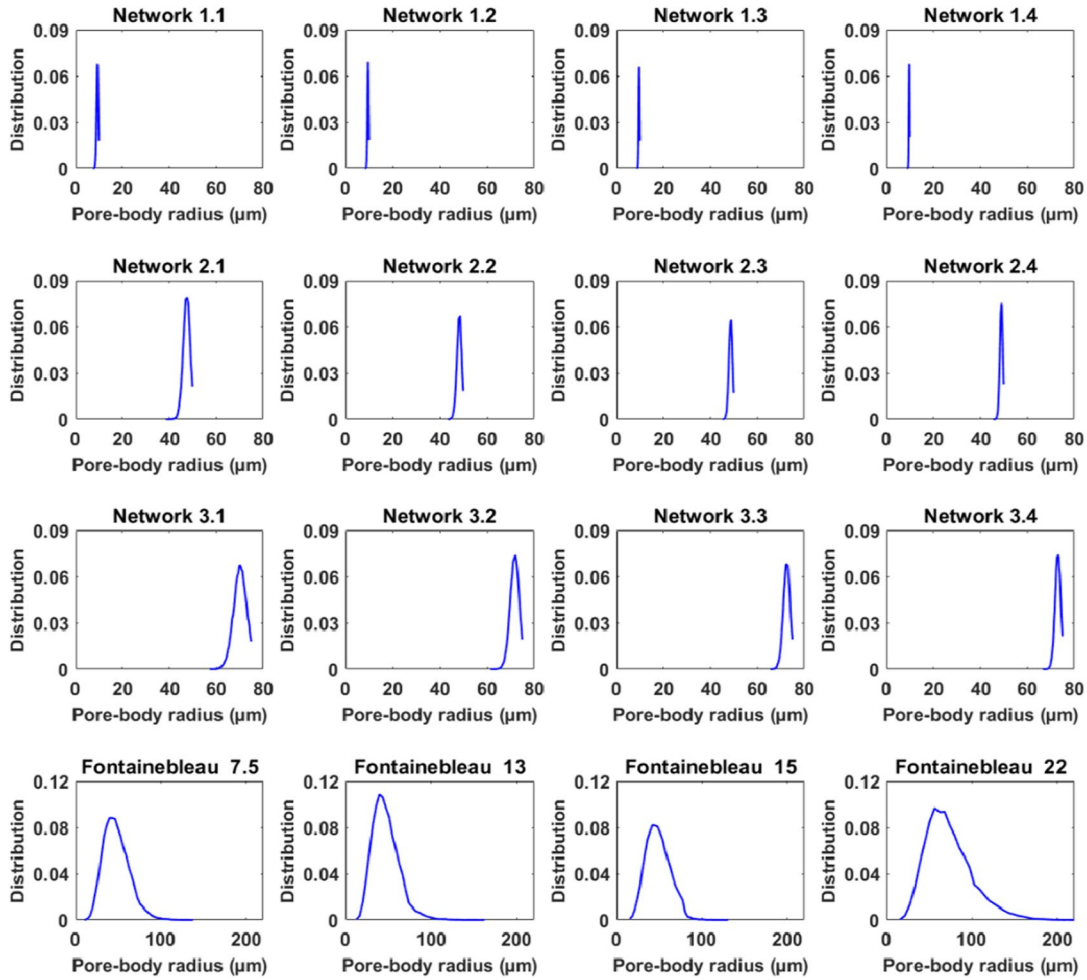


Figure 1. Pore-body radius distributions for 16 pore networks used in this study.

in which i represents each of the pore bodies and j denotes all the pore throats connecting to pore body i . In Equation 9, q_{ij} is the flow rate between two pore bodies that depends on the hydraulic conductance g_{hij} , the distance between the centers of the two pore bodies l_{ij} , and the pressure difference ΔP_{ij} as follows

$$q_{ij} = \frac{g_{hij}}{l_{ij}} \Delta P_{ij} \quad (10)$$

The fluid conductance between two pore bodies was determined using the harmonic mean of contributing conductances

$$\frac{l_{ij}}{g_{hij}} = \frac{l_{bi}}{g_{hi}} + \frac{l_t}{g_{ht}} + \frac{l_{bj}}{g_{hj}} \quad (11)$$

where l_{bi} and l_{bj} represent the distance between the center of a pore body and the interface where the pore body and pore throat meet, and l_t is the pore-throat length (Valvatne, 2004). Assuming laminar flow, the hydraulic conductance of a pore with irregular cross section is given by

$$g_h = c \frac{A_p^2 G}{\mu} \quad (12)$$

in which c is a constant whose value is 0.5 for circular pores, G is the shape factor, and A_p is the pore cross-section. The governing equations for fluid-flow simulation in each pore network with a given pore coordination

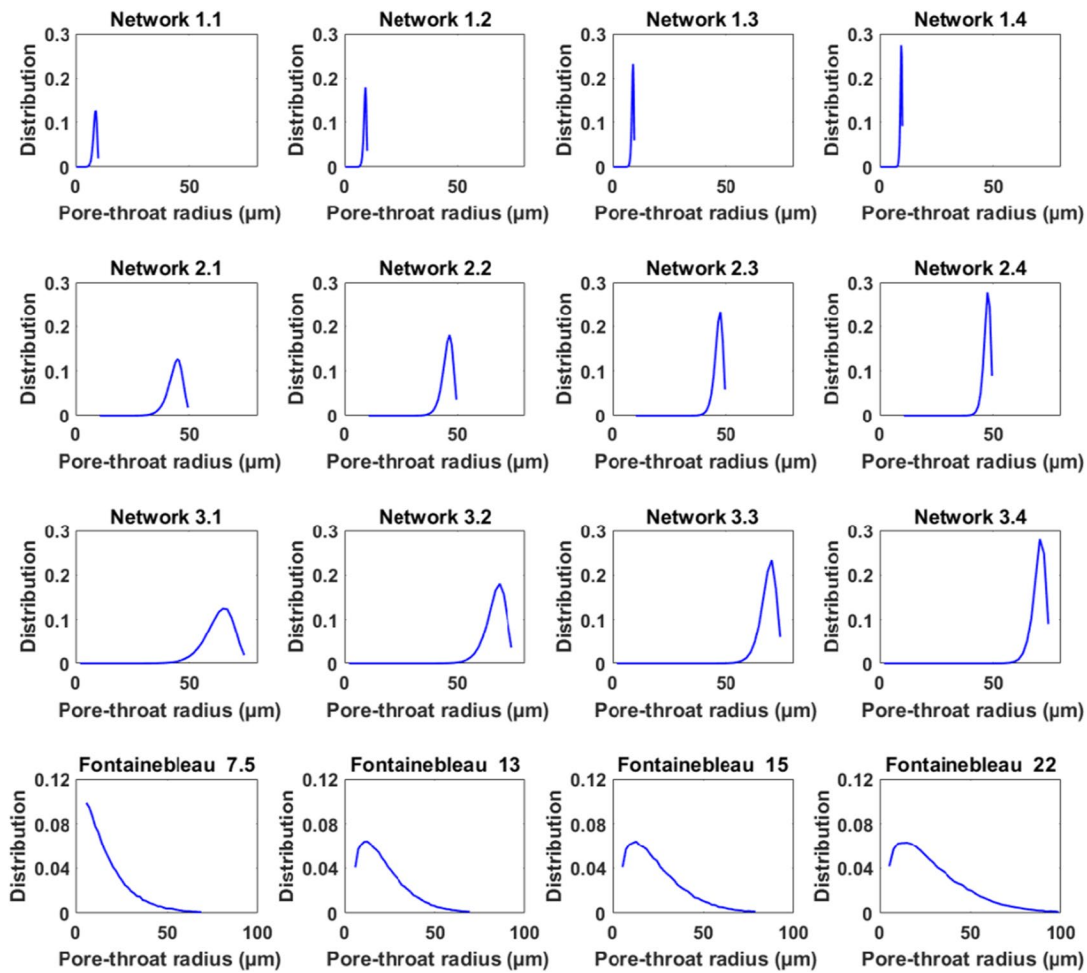


Figure 2. Pore-throat radius distributions for 16 pore networks used in this study.

number were iterated until convergence was reached, after which the permeability was determined by averaging over a hundred realizations.

4.3. Determining the Exponent t

To calculate the exponent t for flow in each pore network, we carried out the simulations at $Z = 1.5$ ($\sim Z_c$), that is, at the percolation threshold in a finite network of size L . We first plotted k against L on a log-log scale and then fitted $k \propto L^{-t/\nu}$ to the data. Since the exponent t/ν is positive, one should expect k to decrease as L increases

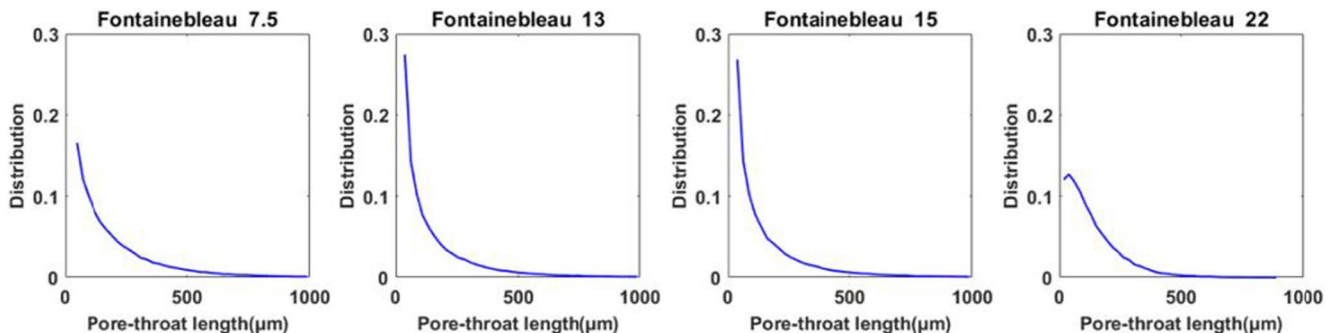


Figure 3. Pore-throat length distributions for four pore networks from Fontainebleau sandstones used in this study.

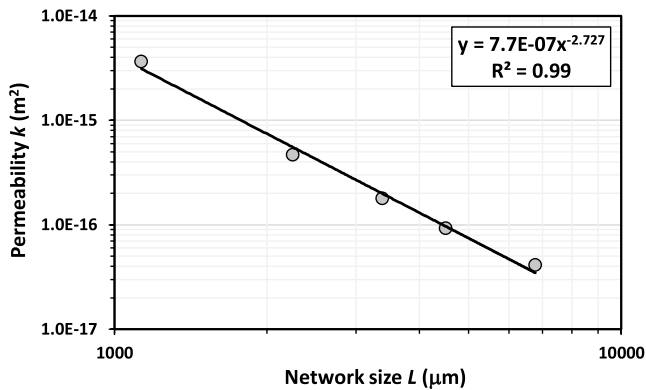


Figure 4. Permeability, k , versus network size, L , at the percolation threshold ($Z = Z_c \sim 1.5$) for the Fontainebleau sandstone with porosity 7.5%, on a double-logarithmic scale. The solid line represents the fitted power law $k \propto L^{-t/\nu}$ with $R^2 = 0.99$. For this pore network, given that $\nu = 0.88$ in three dimensions, we found $t = 2.4$.

at the percolation threshold ($Z \rightarrow Z_c$). Using the universal value of ν in three dimensions, $\nu = 0.88$ (Kozlov & Laguës, 2010; Stauffer & Aharony, 1994), the value of the exponent t was determined from the optimized fit of t/ν . The process is shown for Fontainebleau 7.5 in Figure 4, and the value of t for each pore network is reported in Table 1.

5. Results

In what follows, we present the results of finite-size scaling analysis for each pore network, and show that although the k - L plot, including simulations for various Z values, seem scattered, the data collapse onto a single quasi-universal curve after applying finite-size scaling equation, Equation 5.

5.1. Synthetic Networks1

The results for Network 1 are presented in Figure 5. Our simulations with Networks 1.1 to 1.4 indicated that the permeability increases with network size for $Z = 5$ and 6. Although its value did not vary much with the scale for $Z = 4$, we found that k decreases as network size increases for Z smaller than 4.

Recall that large Z near 6 correspond to large p , the fraction of flow-carrying pores, near 1, whereas small values of Z near 1.5 correspond to p near p_c . We also display the results of finite-size scaling analysis for each pore network in Figure 5. As can be seen, the data, corresponding to the simulations for all coordination numbers, $Z = 1.65, 1.75, 2, 3, 3.25, 3.5, 4, 5$, and 6, collapsed onto a single quasi-universal curve. This means that Equation 5, which is the modified form of the original finite-size scaling equation, Equation 4, is capable of capturing the effect of pore-scale heterogeneity, as reflected in the average pore coordination number Z .

The estimates of t computed for Networks 1.1 to 1.4 vary between 1.46 and 1.64 (Table 1). These values are, however, smaller than the universal value of $t \approx 2$ in three dimensions (Kozlov & Laguës, 2010; Stauffer & Aharony, 1994). The reason why the value of t is less than two in these networks is not clear. Recall that in random networks or those with short-range correlated, one should theoretically expect $t \approx 2$, if the conductance distribution is narrow enough and the first inverse moment is finite (Equation 3); $t < 2$ may occur in networks with long-range correlations (Sahimi, 2011), but that is not the case here, because the correlations are short-ranged in the pore networks that we simulated. Balberg et al. (2016) proposed another explanation for the exponent t being less than its universal value of about 2. The mean number of occupied bonds or pore throats per site of a network at its percolation threshold is $B_c = p_c Z$. Thus, $B = pZ$ varies linearly with p and one may write $k \propto (B - B_c)^t$. Balberg et al. (2016) suggested that in certain percolation network with a broad conductance distribution, B can depend on p sublinearly, which gives rise to measured, or computed through simulation, values of t less than its universal value. Another possible reason for the estimates $t < 2$ is finite-size effects. The pore networks used in our study are not very large, and it is known (Sahimi & Arbabi, 1991) that there are significant correction to scaling when estimating the exponent t by finite-size scaling at the percolation threshold. Their effect can be manifested only when one does simulation with very large networks.

Figure 6 shows the dependence on the network size of the computed permeability for various pore coordination numbers. Similar to the results of Network 1, we found the k - L plots are scattered. However, Equation 5 resulted in collapsed data shown in Figure 6, suggesting that the proposed modified finite-size scaling analysis is still valid for various Z and network sizes. Estimates of t range from 1.77 to 1.84, as shown in Table 1, which is again smaller than the universal value of 2 (Kozlov & Laguës, 2010; Stauffer & Aharony, 1994). More importantly, we find that the permeability of Networks 2.1–2.4 increases with increasing scale only when $Z = 6$. This is not clear in Figure 6 because the permeability is plotted on the logarithmic scale. k remains nearly constant for various network sizes with $Z = 5$. The computed permeabilities for $Z < 5$ indicate, however, a decreasing trend with the scale; see Figure 6.

Figure 7, similar to Figures 5 and 6, shows how the pore coordination number greatly affects the scale dependence of the permeability in Network 3, and that Equation 5 leads to the collapse of the k - L curves onto a single universal curve, validating the modified finite-size scaling analysis. In this case the exponent t varied between 1.77 and 1.88, shown in Table 1, with an average value of 1.83, again smaller than the universal value of two in three dimensions (Stauffer & Aharony, 1994). The results for Network three indicate that the permeability

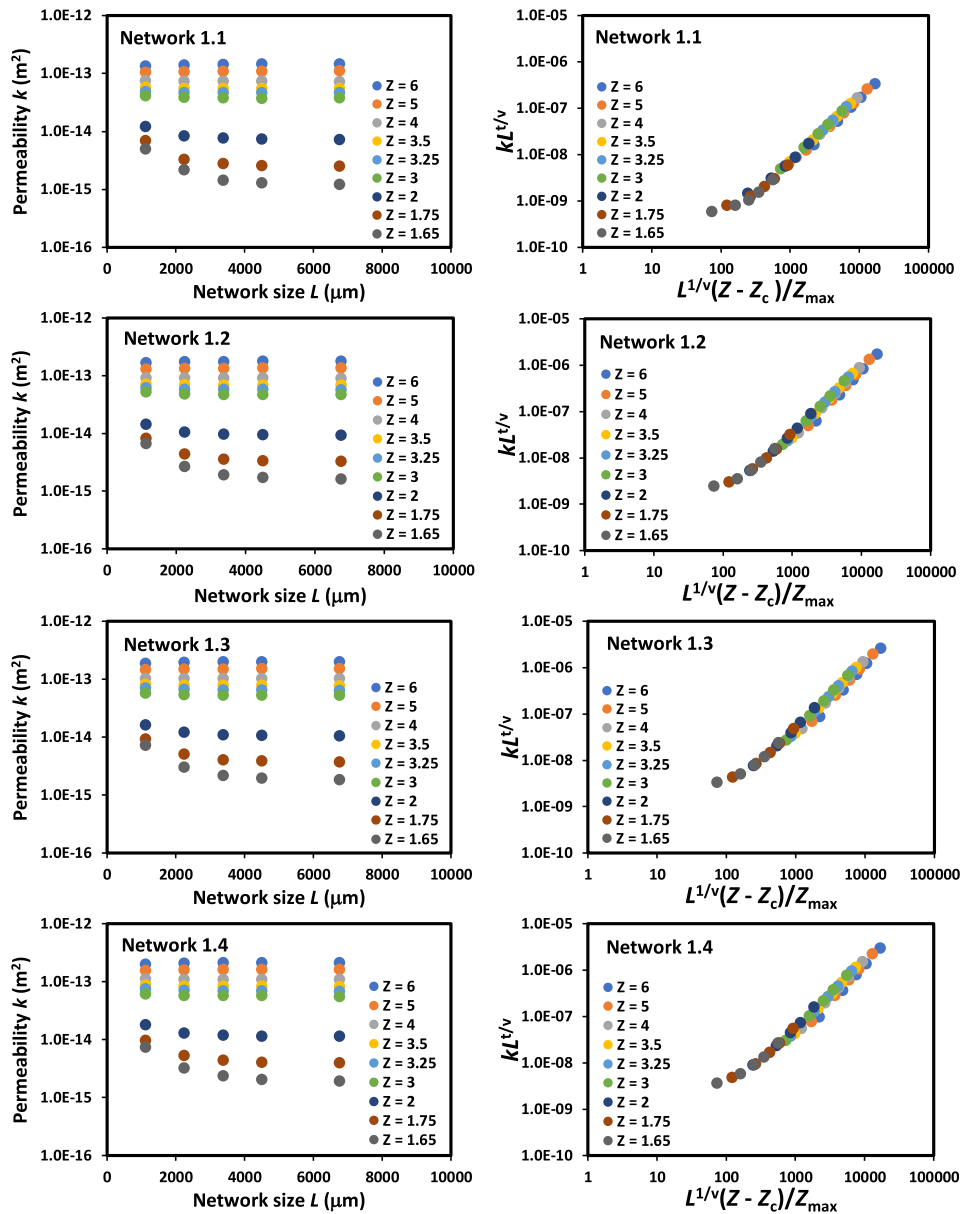


Figure 5. (left) Simulated permeability at various pore coordination numbers versus network size, and (right) the data collapse for Network 1 with $Z_c = 1.5$ and $Z_{max} = 6$.

increases with the increase in the network size for $Z = 6$, but remains almost constant for $Z = 5$, which is similar to Network 2. As Figure 7 indicates, however, k decreases with increasing network size when $Z < 5$. The decrease in the permeability is significant and is near one order of magnitude for $Z = 1.65$, close to the threshold, $Z_c \sim 1.5$. The increasing trend in the scale dependence of the permeability was reported by Esmaeilpour et al. (2021) who simulated flow in Networks 1 to 3 with $Z = 6$ (see their Figures 5–7). They did not, however, utilize finite-size scaling analysis to explain the scale dependence of the permeability in such networks.

5.2. Fontainebleau Sandstones

The results for the permeability of Fontainebleau pore networks are presented in Figure 8. We find that in all the Fontainebleau samples the permeability decreases as the network size increases from 1,130 to 6,770 μm , regardless of Z . This is not consistent with our results for the synthetic networks for which we found a transition in the scale dependence of the permeability. As in Figures 1 and 2, the Fontainebleau pore networks have the broadest

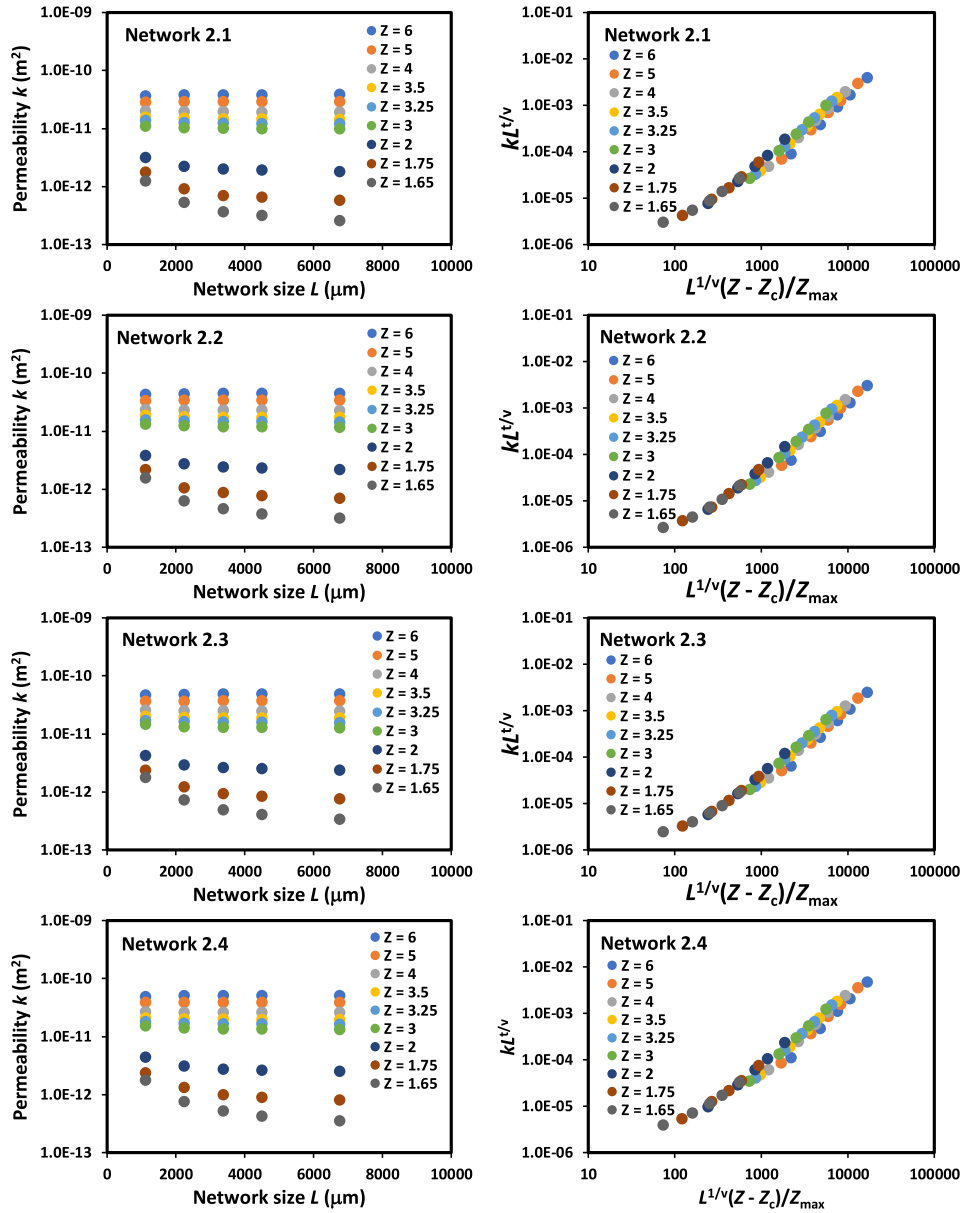


Figure 6. (left) Simulated permeability at various pore coordination numbers versus network size, and (right) the data collapse for Network 2 with $Z_c = 1.5$ and $Z_{max} = 6$.

pore-size distributions among those studied here. This indicates that the presence of the transition might depend on the level of heterogeneity, represented by the broadness of the pore-throat radius distribution, as we discuss in the next section.

Figure 8 also shows the results of finite-size scaling analysis. All the data associated with various Z collapse perfectly using the appropriate t value. Interestingly, the modified finite-size scaling analysis led to more accurate data collapses for Fontainebleau pore networks, representing natural porous media, than the synthetic ones, which can be seen by comparing Figure 8 with Figures 5–7. For pore networks representing the Fontainebleau sandstone, we find t between 2.33 and 2.74 (see Table 1) with an average of 2.52, which is greater than those in synthetic networks.

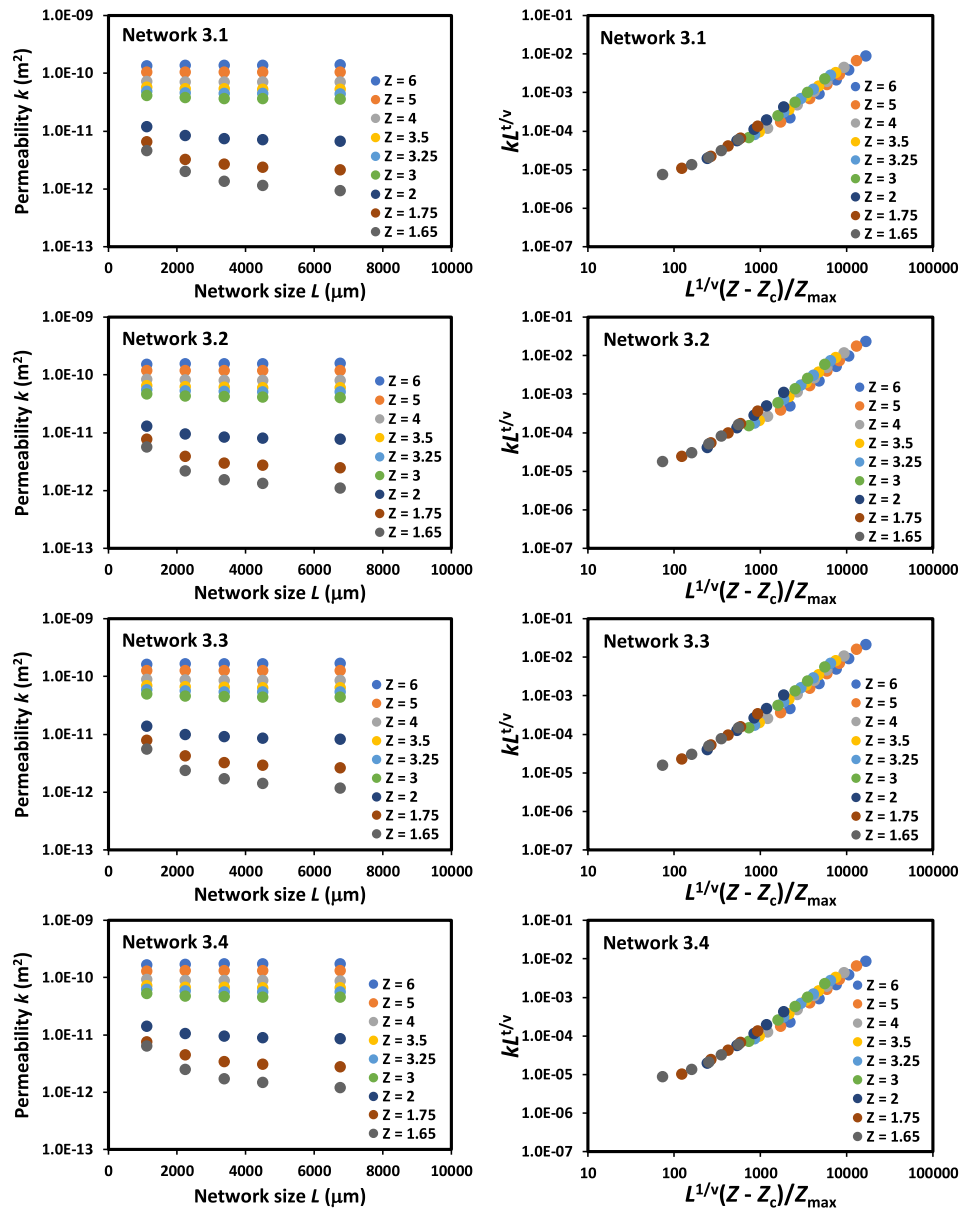


Figure 7. (left) Simulated permeability at various pore coordination numbers versus network size, and (right) the data collapse for Network 3 with $Z_c = 1.5$ and $Z_{max} = 6$.

6. Discussion

The average value of t is 1.58 for Network 1, 1.81 for Network 2, 1.83 for Network 3, and 2.52 for Fontainebleau sandstones. According to the continuum percolation theory (for a review see Balberg, 2021), the exponent t can be a function of the broadness of the conductance or pore-throat radius distribution, as was demonstrated for models of packing of spheres (Feng et al., 1987; Kogut & Straley, 1979). Figure 2 indicates that the pore-throat radius distribution becomes broader from top to bottom, in agreement with the observation that the average t increases from Network 1 to Fontainebleau pore networks.

For Networks 1 to 3, we found $4.2 \times 10^{16} \leq f_{-1} \leq 9.3 \times 10^{22}$ and in Fontainebleau pore networks $5.9 \times 10^{19} \leq f_{-1} \leq 1.3 \times 10^{20}$, which indicate that the exponent t should be nonuniversal ($t \neq 2$) in the pore networks. While the very large values of the first inverse moment of the flow conductance distribution may explain why the exponent t is not universal, the nonuniversal values reported in the past were typically larger than 2.

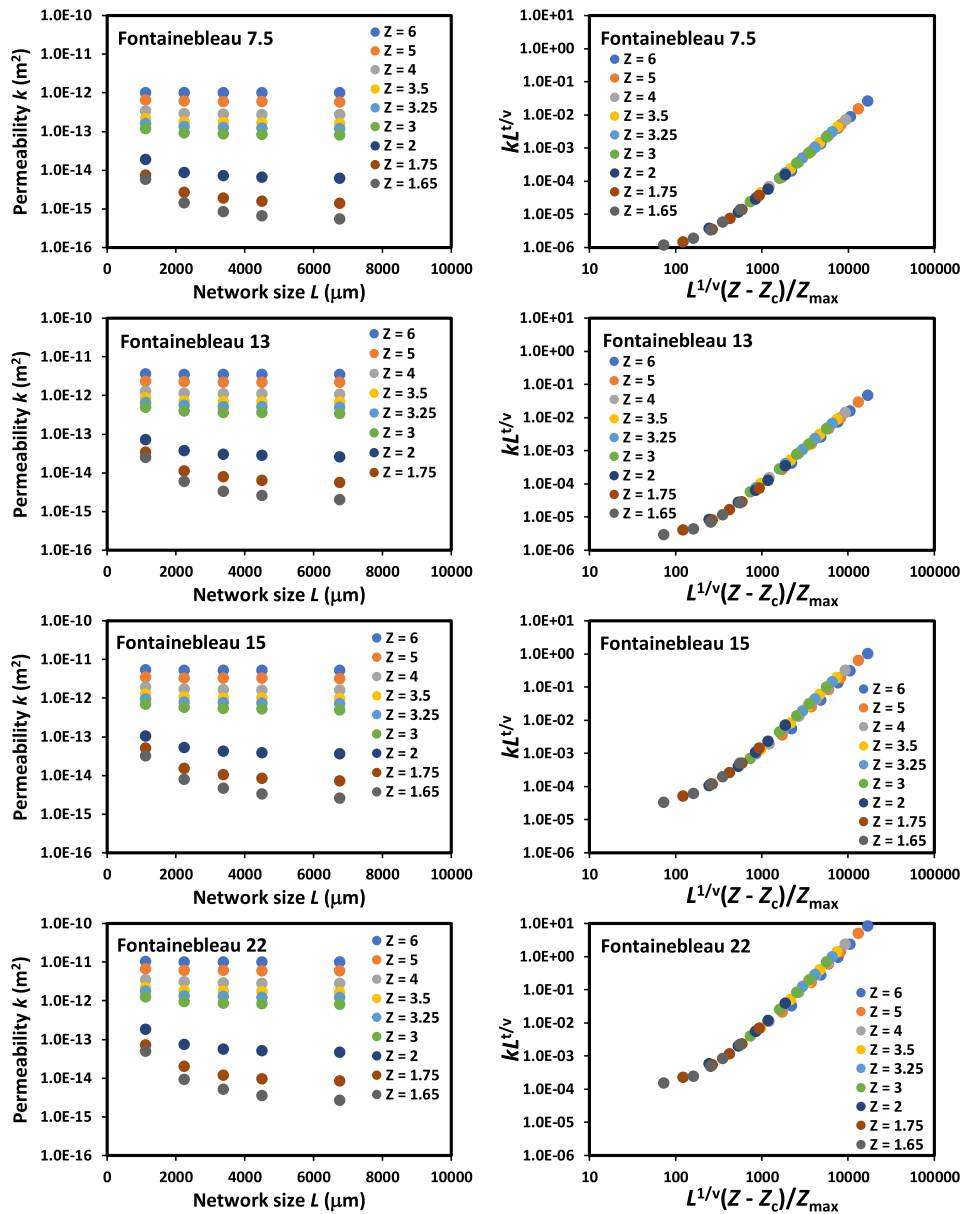


Figure 8. (left) Simulated permeability at various pore coordination numbers versus network size, and (right) the data collapse for Fontainebleau sandstones with $Z_c = 1.5$ and $Z_{max} = 6$.

Therefore, as we stated earlier, it is not completely clear why the exponent t is found to be less than 2, as in the synthetic pore networks. We already offered two possible mechanisms for the estimates of $t < 2$. Another possibility could be due to the pore-throat radius distributions being left-skewed in the synthetic networks, while being right-skewed in the Fontainebleau samples (Figure 2). This implies that the mode of the pore-throat radius distribution occurs at larger pore throats in the synthetic networks. In the Fontainebleau pore networks, however, it happens at smaller pore throats. A fourth possibility could be the truncation of the pore-throat radius distribution, meaning that the minimum pore-throat radius is a finite positive value (see Table 1), albeit very small, instead of approaching zero as presumed by Kogut and Straley (1979) and Feng et al. (1987), although that usually results in the exponent t being larger than 2. Therefore, further investigations are still required to study the effect of skewness and truncation of the pore-throat radius or pore-conductance distribution on the exponent t .

Our results demonstrate clearly that if the small-scale heterogeneities of the network, as reflected in the permeability scaling exponent t and pore coordination number, are accurately captured, the modified finite-size scaling

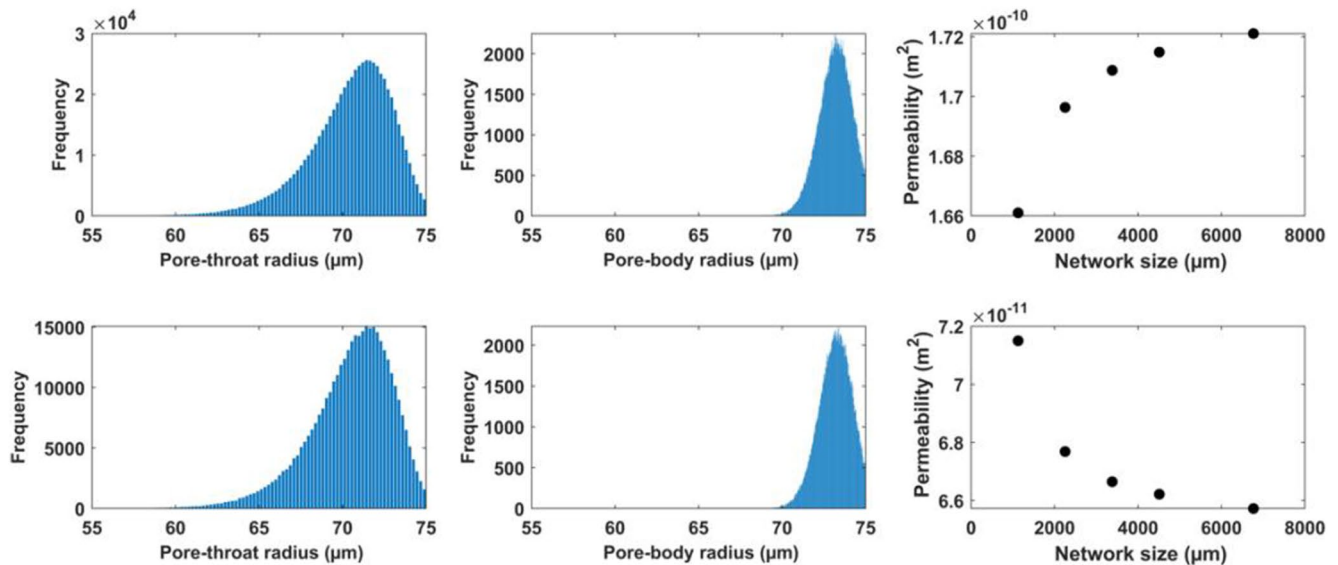


Figure 9. Pore-body and pore-throat size distributions as well as scale-dependent permeability for Network 3.4 with pore coordination number $Z = 6$ (top plots) and 3.5 (bottom plots). Permeability simulations were averaged over a hundred iterations.

analysis, Equation 5, provides a promising framework to accurately scale the data over a wide range of variations in the length scale above the percolation threshold, as shown in Figures 5–8. We find that finite-size scaling analysis is applicable not only near the critical pore coordination number ($Z \rightarrow Z_c$), but also far above that ($Z \rightarrow Z_{\max}$). This is consistent with the results of Sadeghnejad et al. (2010) who investigated the effect of anisotropy on the connectivity and conductivity using the continuum percolation theory. They utilized, however, the original form of the finite-size scaling analysis, Equation 4, to illustrate the collapse of their data. Similar results were reported by Sadeghnejad et al. (2012) for field characterizations of conductivity in geologic formations.

The results demonstrate clearly that there might exist a transition in the scale-dependence of the permeability, depending on the broadness of the pore-throat radius distribution. Such a transition may very well address the contradictory observations reported in the literature, as to whether the permeability should increase or decrease with the increasing length scale. In Network 1 with the narrowest pore-throat radius distribution, the transition happened around $Z = 4$, whereas in Networks 2 and 3 with broader distributions it occurred around $Z = 5$. The Fontainebleau pore networks with the broadest pore-throat size distributions did not, however, exhibit any transition, and their permeability decreased with the network size, regardless of the pore coordination number.

Figure 9 highlights such a transition in the scale dependence of the permeability for Network 3.4. In the top plots, the pore-throat and pore-body radius distributions, as well as the scale dependence of k are shown for $Z = 6$, while the same are shown in the bottom plot for $Z = 3.5$. Although the two pore networks have statistically the same pore-body and pore-throat radius distributions, the permeability increases with the scale for $Z = 6$, whereas it decreases for $Z = 3.5$. These results demonstrate the effect of pore connectivity and small-scale heterogeneity on the scale dependence of the permeability. Bernabé et al. (2003) also simulated fluid flow in pore networks with various levels of heterogeneity. For this purpose, they constructed pore networks in which the pore-throat radius conformed to the log-uniform distribution with coefficient of variations (CVs) 0.06, 0.4, 0.8, 1.2, 1.6, and 1.9. For the square networks, Bernabé et al. (2003) showed that the permeability remained nearly constant as the network size increased in homogeneous networks with $\text{CV} = 0.06$ and 0.4 (see their Figure 1a). When the networks were more heterogeneous (with $\text{CV} > 0.4$), however, their permeability decreased with increasing the network size.

In porous media, the maximum pore coordination number, Z_{\max} , can be as large as 10 for example, in Berea sandstones (Dong & Blunt, 2009), dolomites (Moaddel et al., 2018), and limestones (Ebrahimi et al., 2013) or even 20, for example, in Fontainebleau sandstones (Lindquist et al., 2000) and glass bead packs (Yanuka et al., 1986). However, the average pore coordination number Z always stays around 3–4 (Blunt, 2017; Liang et al., 2000; Vogel & Roth, 2001). This makes the ratio $Z/Z_{\max}(p)$ close to $Z_c/Z_{\max}(p_c)$ and, thus, implying that the porous media are near their percolation thresholds. Recall that the critical pore coordination number in three dimensions is

~ 1.5 . This means that Equations 1 and 2, as well as other power-law relationships of percolation theory that are theoretically valid above and near the percolation threshold, should be applicable to soils and rocks, as shown by Hunt et al. (2014), a result anticipated much earlier by Sahimi (1993).

Although our present study was limited to laboratory-scale porous materials, the same approach may be applied to media at much larger scales. In a field-scale porous medium, for example, the spatial distribution of the block-scale permeabilities vary over orders of magnitude. Thus, although the percolation effect may not be obvious at the first glance, it does actually exist, since a finite fraction of the local permeabilities may be very small and, therefore, contribute very little to the overall fluid flow process. This was already hinted at in the early simulations of flow and transport in field-scale porous media (for a discussion of this issue see Sahimi, 2011). Such simulations indicated that only a small fraction of all the pores or bond in the network contribute significantly to the fluid flow process, which implies a percolation effect, even at field scale. Work in this direction is in progress.

7. Conclusions

To study the effect of length scale on the permeability, we simulated fluid flow in pore networks with various levels of pore-scale heterogeneity, represented by the pore-throat radius distribution and pore coordination number. We modified the original form of the finite-size scaling analysis to rescale the k - L data for various average pore coordination numbers, $Z = 1.5, 1.65, 1.75, 2, 3, 3.25, 3.5, 4, 5,$ and 6 . The results demonstrated that the proposed finite-size scaling form accurately collapses data onto a single quasi-universal curve in each pore network, although the k - L plot was scattered. We also found that depending on the broadness of pore-throat radius distribution, the trends of increasing permeability with the scale may crossover to the decreasing behavior as the average pore coordination number decreases. Further investigations are required to study the scale dependence of permeability on rock/soil images.

Data Availability Statement

The pore-network simulations are available at: <http://www.hydroshare.org/resource/e3c1e6a8a9f04f90b8bc73d-fd846bb02>.

Acknowledgment

Behzad Ghanbarian acknowledges Kansas State University for supports through faculty startup funds. Misagh Esmailpour is grateful to the College of Arts and Sciences as well as Graduate Students Council at Kansas State University for Travel Awards.

References

- Arns, C. H., Knackstedt, M. A., Pinczewski, W. V., & Garboczi, E. (2002). Computation of linear elastic properties from microtomographic images: Methodology and agreement between theory and experiment. *Geophysics*, *67*, 1396–1405. <https://doi.org/10.1190/1.1512785>
- Arns, C. H., Knackstedt, M. A., Pinczewski, W. V., & Lindquist, W. B. (2001). Accurate computation of transport properties from microtomographic images. *Geophysical Research Letters*, *28*, 3361–3364. <https://doi.org/10.1029/2001gl012987>
- Aslannejad, H., Hassanizadeh, S. M., Raoof, A., de Winter, D. A. M., Tomozeiu, N., & van Genuchten, M. T. (2017). Characterizing the hydraulic properties of paper coating layer using FIB-SEM tomography and 3D pore-scale modeling. *Chemical Engineering Science*, *160*, 275–280. <https://doi.org/10.1016/j.ces.2016.11.021>
- Avseth, P., Mukerji, T., & Mavko, G. (2010). *Quantitative seismic interpretation: Applying rock physics tools to reduce interpretation risk*. Cambridge University Press.
- Balberg, I. (2021). In M. Sahimi, & A. G. Hunt (Eds.).
- Balberg, I., Azulay, D., Goldstein, Y., & Jedrzejewski, J. (2016). Possible origin of the smaller-than-universal percolation-conductivity exponent in the continuum. *Physical Review E*, *93*, 062132. <https://doi.org/10.1103/physreve.93.062132>
- Bernabé, Y., Bruderer-Weng, C., & Maineult, A. (2003). Permeability fluctuations in heterogeneous networks with different dimensionality and topology. *Journal of Geophysical Research: Solid Earth*, *108*(B7), 2351. <https://doi.org/10.1029/2002JB002326>
- Bernabé, Y., Li, M., & Maineult, A. (2010). Permeability and pore connectivity: A new model based on network simulations. *Journal of Geophysical Research: Solid Earth*, *115*(10), 1–14. <https://doi.org/10.1029/2010JB007444>
- Blunt, M. J. (2017). *Multiphase Flow in Permeable Media*. Cambridge University Press. <https://doi.org/10.1017/9781316145098>
- Blunt, M. J., Bijeljic, B., Dong, H., Gharbi, O., Iglauer, S., & Mostaghimi, P. (2013). Pore-scale imaging and modelling. *Advances in Water Resources*, *51*, 197–216. <https://doi.org/10.1016/j.advwatres.2012.03.003>
- Chen, Y., Wei, L., Mastalerz, M., & Schimmelmann, A. (2015). The effect of analytical particle size on gas adsorption porosimetry of shale. *International Journal of Coal Geology*, *138*, 103–112. <https://doi.org/10.1016/j.coal.2014.12.012>
- Cnudde, V., & Boone, M. N. (2013). High-resolution X-ray computed tomography in geosciences: A review of the current technology and applications. *Earth-Science Reviews*, *123*, 1–17. <https://doi.org/10.1016/j.earscirev.2013.04.003>
- Crook, N., Binley, A., Knight, R., Robinson, D. A., Zarnetske, J., & Haggerty, R. (2008). Electrical resistivity imaging of the architecture of substream sediments. *Water Resources Research*, *44*(4), W00D13. <https://doi.org/10.1029/2008wr006968>
- Das, D. B., & S. M. Hassanizadeh (Eds.). (2005). *Upscaling multiphase flow in porous media*. Springer.
- Davudov, D., & Moghanloo, R. G. (2018). Scale-Dependent Pore and Hydraulic Connectivity of Shale Matrix. *Energy & Fuels*, *32*, 99–106. <https://doi.org/10.1021/acs.energyfuels.7b02619>
- Dong, H., & Blunt, M. J. (2009). Pore-network extraction from micro-computerized-tomography images. *Physical Review E - Statistical, Nonlinear and Soft Matter Physics*, *80*(3), 1–11. <https://doi.org/10.1103/PhysRevE.80.036307>

- Duda, A., Koza, Z., & Matyka, M. (2011). Hydraulic tortuosity in arbitrary porous media flow. *Physical Review E - Statistical, Nonlinear and Soft Matter Physics*, 84(3), 1–8. <https://doi.org/10.1103/PhysRevE.84.036319>
- Ebrahimi, A. N., Jamshidi, S., Iglauer, S., & Boozarjomehry, R. B. (2013). Genetic algorithm-based pore network extraction from micro-computed tomography images. *Chemical Engineering Science*, 92, 157–166. <https://doi.org/10.1016/j.ces.2013.01.045>
- Esmailpour, M. (2021). *Scale-dependent petrophysical properties in porous media: A pore-network study*. MSc thesis. Kansas State University.
- Esmailpour, M., Ghanbarian, B., Liang, F., & Liu, H. H. (2021). Scale-dependent permeability and formation factor in porous media: Applications of percolation theory. *Fuel*, 301, 121090. <https://doi.org/10.1016/j.fuel.2021.121090>
- Ewing, R. P., Hu, Q., & Liu, C. (2010). Scale dependence of intragranular porosity, tortuosity, and diffusivity. *Water Resources Research*, 46(6), 1–12. <https://doi.org/10.1029/2009WR008183>
- Feng, S., Halperin, B. I., & Sen, P. N. (1987). Transport properties of continuum systems near the percolation threshold. *Physical Review B*, 35(1), 197–214. <https://doi.org/10.1103/PhysRevB.35.197>
- Fisher, M. E. (1971). The theory of critical point singularities. In M. S. Green (Ed.), *Critical Phenomena*. Academic Press.
- Garbesi, K., Sextro, R. G., Robinson, A. L., Wooley, J. D., Owens, J. A., & Nazaroff, W. W. (1996). Scale dependence of soil permeability to air: Measurement method and field investigation. *Water Resources Research*, 32, 547–560. <https://doi.org/10.1029/95wr03637>
- Ghanbarian, B., Hunt, A. G., Sahimi, M., Ewing, R. P., & Skinner, T. E. (2013). Percolation theory generates a physically based description of tortuosity in saturated and unsaturated porous media. *Soil Science Society of America Journal*, 77(6), 1920. <https://doi.org/10.2136/sssaj2013.01.0089>
- Ghanbarian, B., Taslimitehrani, V., Dong, G., & Pachepsky, Y. A. (2015). Sample dimensions effect on prediction of soil water retention curve and saturated hydraulic conductivity. *Journal of Hydrology*, 528, 127–137. <https://doi.org/10.1016/j.jhydrol.2015.06.024>
- Ghanbarian, B., Taslimitehrani, V., & Pachepsky, Y. A. (2017). Accuracy of sample dimension-dependent pedotransfer functions in estimation of soil saturated hydraulic conductivity. *Catena*, 149, 374–380. <https://doi.org/10.1016/j.catena.2016.10.015>
- Ghanbarian-Alavijeh, B., Skinner, T. E., & Hunt, A. G. (2012). Saturation dependence of dispersion in porous media. *Physical Review E - Statistical, Nonlinear and Soft Matter Physics*, 86(6), 1–14. <https://doi.org/10.1103/PhysRevE.86.066316>
- Gupta, V. K., I. Rodríguez-Iturbe, & E. F. Wood (Eds.), (2012). *Scale problems in hydrology: Runoff generation and basin response* (Vol. 6). Springer Science & Business Media.
- Han, H., Cao, Y., Chen, S. J., Lu, J. G., Huang, C. X., Zhu, H. H., et al. (2016). Influence of particle size on gas-adsorption experiments of shales: An example from a Longmaxi Shale sample from the Sichuan Basin, China. *Fuel*, 186, 750–757. <https://doi.org/10.1016/j.fuel.2016.09.018>
- Hewett, T. A. (1986). Fractal distributions of reservoir heterogeneity and their influence on fluid transport. In *SPE Annual Technical Conference and Exhibition, New Orleans, Louisiana*. (p. SPE-15386-MS). <https://doi.org/10.2118/15386-ms>
- Hirsch, L. M., & Thompson, A. H. (1994). Size-dependent scaling of capillary invasion including buoyancy and pore size distribution effects. *Physical Review E*, 50(3), 2069–2086. <https://doi.org/10.1103/PhysRevE.50.2069>
- Hopmans, J. W., Nielsen, D. R., & Bristow, K. L. (2002). How useful are small-scale soil hydraulic property measurements for large-scale vadose zone modeling. In D. Smiles, P. A. C. Raats, & A. Warrick (Eds.), *In Heat and mass Transfer in the natural Environment, AGU, geophysical Monograph Series No 129* (pp. 247–258). <https://doi.org/10.1029/129gm20>
- Hubbard, S. S., Rubin, Y., & Majer, E. (1997). Ground-penetrating-radar-assisted saturation and permeability estimation in bimodal systems. *Water Resources Research*, 33(5), 971–990. <https://doi.org/10.1029/96WR03979>
- Hunt, A., Ewing, R., & Ghanbarian, B. (2014). *Percolation theory for flow in porous media*.
- Hunt, A. G., & Sahimi, M. (2017). Transport and reaction in porous media: Percolation scaling, critical-path analysis, and effective-medium approximation. *Reviews of Geophysics*, 55, 993–1078. <https://doi.org/10.1002/2017RG000558>
- Jerauld, G. R., Hatfield, J. C., Scriven, L. E., & Davis, H. T. (1984). Percolation and conduction on Voronoi and triangular networks: A case study in topological disorder. *Journal of Physics C: Solid State Physics*, 17(9), 1519–1529. <https://doi.org/10.1088/0022-3719/17/9/010>
- Ji, L., Zhang, T., Milliken, K. L., Qu, J., & Zhang, X. (2012). Experimental investigation of main controls to methane adsorption in clay-rich rocks. *Applied Geochemistry*, 27, 2533–2545. <https://doi.org/10.1016/j.apgeochem.2012.08.027>
- Jury, W. A., Or, D., Pachepsky, Y., Vereecken, H., Hopmans, J. W., Ahuja, L. R., et al. (2011). Kirkham's legacy and contemporary challenges in soil physics research. *Soil Science Society of America Journal*, 75, 1589–1601. <https://doi.org/10.2136/sssaj2011.0115>
- Kalma, J. D., & M. Sivapalan (Eds.), (1995). *Scale issues in hydrological modelling*. John Wiley and Sons.
- Kirkpatrick, S. (1979). Models of disordered materials. In R. Balian, R. Maynard, & G. Toulouse (Eds.), *Ill-condensed Matter* (pp. 321–403).
- Kirsch, R. (Ed.), (2006). *Groundwater Geophysics: A Tool for Hydrogeology*. Springer.
- Kogut, P. M., & Straley, J. P. (1979). Distribution-induced non-universality of the percolation conductivity exponents. *Journal of Physics C: Solid State Physics*, 12(11), 2151–2159. <https://doi.org/10.1088/0022-3719/12/11/023>
- Kozlov, B., & Laguës, M. (2010). Universality of 3D percolation exponents and first-order corrections to scaling for conductivity exponents. *Physica A: Statistical Mechanics and its Applications*, 389, 5339–5346. <https://doi.org/10.1016/j.physa.2010.08.002>
- Larson, R. G., & Morrow, N. R. (1981). Effects of sample size on capillary pressures in porous media. *Powder Technology*, 30(2), 123–138. [https://doi.org/10.1016/0032-5910\(81\)80005-8](https://doi.org/10.1016/0032-5910(81)80005-8)
- Liang, Z., Ioannidis, M. A., & Chatzis, I. (2000). Geometric and topological analysis of three-dimensional porous media: Pore space partitioning based on morphological skeletonization. *Journal of Colloid and Interface Science*, 221(1), 13–24. <https://doi.org/10.1006/jcis.1999.6559>
- Lindquist, W. B., Venkatarangan, A., Dunsmuir, J., & Wong, T. F. (2000). Pore and throat size distributions measured from synchrotron X-ray tomographic images of Fontainebleau sandstones. *Journal of Geophysical Research: Solid Earth*, 105(B9), 21509–21527. <https://doi.org/10.1029/2000jb900208>
- Lunt, I. A., Hubbard, S. S., & Rubin, Y. (2005). Soil moisture content estimation using ground-penetrating radar reflection data. *Journal of Hydrology*, 307(1–4), 254–269. <https://doi.org/10.1016/j.jhydrol.2004.10.014>
- Masihi, M., King, P., & Nurafza, P. (2008). Connectivity prediction in fractured reservoirs with variable fracture size: Analysis and validation. *SPE Journal*, 13(1), 12–15. <https://doi.org/10.2118/100229-PA>
- Masihi, M., & King, P. R. (2007). A correlated fracture network: Modeling and percolation properties. *Water Resources Research*, 43(7), 1–9. <https://doi.org/10.1029/2006WR005331>
- Matyka, M., Khalili, A., & Koza, Z. (2008). Tortuosity-porosity relation in porous media flow. *Physical Review E - Statistical, Nonlinear and Soft Matter Physics*, 78(2), 1–8. <https://doi.org/10.1103/PhysRevE.78.026306>
- Moaddel, A., Mütter, D., Gooya, R., Sørensen, H. O., & Stipp, S. L. S. (2018). A fuzzy logic based algorithm for defining and extracting pore network structure from tomography images of rocks. *Advances in Water Resources*, 119, 197–209. <https://doi.org/10.1016/j.advwatres.2018.07.011>
- Navarre-Sitchler, A., & Brantley, S. (2007). Basalt weathering across scales. *Earth and Planetary Science Letters*, 261(1–2), 321–334. <https://doi.org/10.1016/j.epsl.2007.07.010>

- Neuman, S. P. (1994). Generalized scaling of permeabilities: Validation and effect of support scale. *Geophysical Research Letters*, 21(5), 349–352. <https://doi.org/10.1029/94GL00308>
- Neuman, S. P. (2005). Trends, prospects and challenges in quantifying flow and transport through fractured rocks. *Hydrogeology Journal*, 13(1), 124–147. <https://doi.org/10.1007/s10040-004-0397-2>
- Pachepsky, Y., D. E. Radcliffe, & H. M. Selim (Eds.), (2003). *Scaling methods in soil physics*. CRC press.
- Pachepsky, Y. A., Guber, A. K., Yakirevich, A. M., McKee, L., Cady, R. E., & Nicholson, T. J. (2014). Scaling and pedotransfer in numerical simulations of flow and transport in soils. *Vadose Zone Journal*, 13(12). <https://doi.org/10.2136/vzj2014.02.0020>
- Pastewka, L., Prodanov, N., Lorenz, B., Müser, M. H., Robbins, M. O., & Persson, B. N. (2013). Finite-size scaling in the interfacial stiffness of rough elastic contacts. *Physical Review E*, 87, 062809. <https://doi.org/10.1103/physreve.87.062809>
- Petrovitch, C. L., Nolte, D. D., & Pyrak-Nolte, L. J. (2013). Scaling of fluid flow versus fracture stiffness. *Geophysical Research Letters*, 40, 2076–2080. <https://doi.org/10.1002/grl.50479>
- Pyrak-Nolte, L. J., & Nolte, D. D. (2016). Approaching a universal scaling relationship between fracture stiffness and fluid flow. *Nature Communications*, 7, 1–6. <https://doi.org/10.1038/ncomms10663>
- Qian, J., Zhan, H., Luo, S., & Zhao, W. (2007). Experimental evidence of scale-dependent hydraulic conductivity for fully developed turbulent flow in a single fracture. *Journal of Hydrology*, 339, 206–215. <https://doi.org/10.1016/j.jhydrol.2007.03.015>
- Rehfeldt, K. R., Boggs, J. M., & Gelhar, L. W. (1992). Field study of dispersion in a heterogeneous aquifer: 3. Geostatistical analysis of hydraulic conductivity. *Water Resources Research*, 28(12), 3309–3324. <https://doi.org/10.1029/92wr01758>
- Rovey, C. W., & Cherkauer, D. S. (1995). Scale Dependency of Hydraulic Conductivity Measurements. *Groundwater*, 33(5), 769–780. <https://doi.org/10.1111/j.1745-6584.1995.tb00023.x>
- Sadeghnejad, S., Masihi, M., King, P. R., Shojaei, A., & Pishvaei, M. (2010). Effect of anisotropy on the scaling of connectivity and conductivity in continuum percolation theory. *Physical Review E - Statistical, Nonlinear and Soft Matter Physics*, 81(6), 1–5. <https://doi.org/10.1103/PhysRevE.81.061119>
- Sadeghnejad, S., Masihi, M., Shojaei, A., Pishvaei, M., & King, P. R. (2012). Field scale characterization of geological formations using percolation theory. *Transport in Porous Media*, 92(2), 357–372. <https://doi.org/10.1007/s11242-011-9907-6>
- Sahimi, M. (1993). Fractal and superdiffusive transport and hydrodynamic dispersion in heterogeneous porous media. *Transport in Porous Media*, 13(1), 3–40. <https://doi.org/10.1007/BF00613269>
- Sahimi, M. (1994). *Applications of percolation theory*. Taylor and Francis.
- Sahimi, M. (2011). *Flow and transport in porous media and fractured rock* (2nd ed.). Wiley-VCH.
- Sahimi, M., & Arbabi, S. (1991). On correction to scaling for two- and three-dimensional scalar and vector percolation. *Journal of Statistical Physics*, 62, 453. <https://doi.org/10.1007/bf01020881>
- Sahimi, M., Hughes, B. D., Scriven, L. E., & Davis, H. T. (1983a). Critical exponent of percolation conductivity by finite-size scaling. *Journal of Physics C: Solid State Physics*, 16, L521–L527. <https://doi.org/10.1088/0022-3719/16/16/004>
- Sahimi, M., Hughes, B. D., Scriven, L. E., & Davis, H. T. (1983b). Stochastic transport in disordered systems. *The Journal of Chemical Physics*, 78(11), 6849–6864. <https://doi.org/10.1063/1.444631>
- Sahimi, M., Hughes, B. D., Scriven, L. E., & Davis, H. T. (1986). Dispersion in flow through porous media-I. One-phase flow. *Chemical Engineering Science*, 41(8), 2103–2122. [https://doi.org/10.1016/0009-2509\(86\)87128-7](https://doi.org/10.1016/0009-2509(86)87128-7)
- Sahimi, M., & A. G. Hunt (Eds.), (2021). *Complex systems and percolation theory*. Springer.
- Schulze-Makuch, D., Carlson, D. A., Cherkauer, D. S., & Malik, P. (1999). Scale dependency of hydraulic conductivity in heterogeneous media. *Ground Water*, 37, 904–919. <https://doi.org/10.1111/j.1745-6584.1999.tb01190.x>
- Sposito, G. (Ed.), (2008). *Scale dependence and scale invariance in hydrology* (p. 432). Cambridge University Press.
- Stauffer, D., & Aharony, A. (1994). *Introduction to percolation theory* (2nd ed.). Taylor and Francis.
- Sudicky, E. A. (1986). A natural gradient experiment on solute transport in a sand aquifer: Spatial variability of hydraulic conductivity and its role in the dispersion process. *Water Resources Research*, 22(13), 2069–2082. <https://doi.org/10.1029/wr022i013p02069>
- Tinni, A., Fathi, E., Agarwal, R., Sondergeld, C. H., Akkutlu, I. Y., & Rai, C. S. (2012). Shale permeability measurements on plugs and crushed samples. In *SPE Canadian Unconventional Resources Conference* (p. SPE162235). Society of Petroleum Engineers. <https://doi.org/10.2118/162235-ms>
- Valvatne, P. H. (2004). *Predictive pore-scale modelling of multiphase flow*. Imperial College London.
- Vanderborght, J., Kemna, A., Hardelauf, H., & Vereecken, H. (2005). Potential of electrical resistivity tomography to infer aquifer transport characteristics from tracer studies: A synthetic case study. *Water Resources Research*, 41(6), W06013. <https://doi.org/10.1029/2004wr003774>
- Vogel, H. J., & Roth, K. (2001). Quantitative morphology and network representation of soil pore structure. *Advances in Water Resources*, 24(3–4), 233–242. [https://doi.org/10.1016/S0309-1708\(00\)00055-5](https://doi.org/10.1016/S0309-1708(00)00055-5)
- Vysotsky, V. A., Gordon, S. B., Frisch, H. L., & Hammersley, J. M. (1961). Critical percolation probabilities (bond problem). *Physical Review*, 123(5), 1566–1567. <https://doi.org/10.1103/PhysRev.123.1566>
- Wheatcraft, S. W., & Tyler, S. W. (1988). An explanation of scale-dependent dispersivity in heterogeneous aquifers using concepts of fractal geometry. *Water Resources Research*, 24, 566–578. <https://doi.org/10.1029/wr024i004p00566>
- Wildenschild, D., & Sheppard, A. P. (2013). X-ray imaging and analysis techniques for quantifying pore-scale structure and processes in subsurface porous medium systems. *Advances in Water Resources*, 51, 217–246. <https://doi.org/10.1016/j.advwatres.2012.07.018>
- Yanuka, M., Dullien, F. A. L., & Elrick, D. E. (1986). Percolation processes and porous media: I. Geometrical and topological model of porous media using a three-dimensional joint pore size distribution. *Journal of Colloid and Interface Science*, 112, 24–41. [https://doi.org/10.1016/0021-9797\(86\)90066-4](https://doi.org/10.1016/0021-9797(86)90066-4)
- Yoon, H., & Dewers, T. A. (2013). Nanopore structures, statistically representative elementary volumes, and transport properties of chalk. *Geophysical Research Letters*, 40, 4294–4298. <https://doi.org/10.1002/grl.50803>